THE ASTROPHYSICAL JOURNAL, 495:413–423, 1998 March 1

MATTER MIXING FROM AXISYMMETRIC SUPERNOVA EXPLOSION

SHIGEHIRO NAGATAKI,[1,2] TETSUYA M. SHIMIZU,[2] AND KATSUHIKO SATO[1,3]
Received 1997 March 6; accepted 1997 October 8

ABSTRACT

The growth of Rayleigh-Taylor instabilities under axisymmetric explosion is investigated by two-dimensional hydrodynamical calculations. The degree of the axisymmetric explosion and amplitude of the initial perturbation are varied parametrically to find the most favorable parameter for reproducing the observed line profile of heavy elements. It is found that spherical explosion cannot produce ^{56}Ni travelling at high velocity ($\sim$3000 km s^{-1}), the presence of which is affirmed by observation, even if the amplitude of initial perturbation is as large as 30%. On the other hand, strong axisymmetric explosion models produce too much high-velocity ^{56}Ni. Weak axisymmetric explosion is favored for the reproduction of the observed line profile. We believe that this result shows the upper limit of the degree of axisymmetric explosion. This fact will be important for the simulation of collapse-driven supernovae, including rotation, magnetic field, and axisymmetric neutrino radiation, which can potentially cause axisymmetric supernova explosion. In addition, the origin of such a large perturbation does not seem to be the structure of the progenitor but the dynamics of the core collapse explosion itself, since small perturbation cannot produce the high-velocity element, even if axisymmetric explosion models are adopted.

Subject headings: hydrodynamics — nuclear reactions, nucleosynthesis, abundances — supernovae: general — supernovae: individual (SN 1987A)

1. INTRODUCTION

SN 1987A in the Large Magellanic Cloud has provided us with apparent evidence of large-scale mixing in ejecta for the first time. For example, the unexpected early detection of X-rays (Dotani et al. 1987; Sunyaev et al. 1987; Wilson et al. 1988) and gamma rays (Matz et al. 1988) suggests that the radioactive nuclei, which are synthesized at the bottom of the ejecta, are mixed up to the outer layer. The form of the X-ray light curve is also thought to be indirect evidence of mixing and clumping of the heavy elements (e.g., Itoh et al. 1987; Kumagai et al. 1988). Moreover, it is reported that a part of heavy elements, such as Fe II, Ni II, Ar II, and Co II, is mixed up to the fast moving ($\sim$3000–4000 km s^{-1}) outer layers from the observation of the width of infrared spectral lines (Erickson et al. 1988). On the other hand, hydrogen, which has an expansion velocity as low as 800 km s^{-1}, is observed (Höflich 1988).

At present, the growth of Rayleigh-Taylor (R-T) instability is thought to be the most promising mechanism for the explanation of the matter mixing. Although the idea that the instability grows during explosion in Type II supernovae was not new (e.g., Falk & Arnett 1973; Chevalier 1976; Bandiera 1984), it was necessary to calculate numerically the growth of the instability using realistic stellar models in multiple dimensions to see its effect quantitatively. With the improvement of the supercomputer, many people have made such calculations. Early two-dimensional simulations of the first few hr of the explosion showed that the R-T instabilities do indeed grow (Arnett, Fryxell, & Müller 1989; Hachisu et al. 1990; Müller, Fryxell, & Arnett 1990, 1991; Fryxell, Arnett, & Müller 1991).

However, there are some points that are still open to argument. For example, the location and amplitude of the seed of the R-T instability are still unknown. Up to the present two candidates have been proposed for that seed. One is that it is produced by convection during the stellar evolution. It is reported that the density fluctuation $\delta\rho/\rho$ will be $\sim$5% (up to 8%) at the beginning of the core collapse (Bazan & Arnett 1994; Bazan & Arnett 1997) at the inner and outer boundaries of the convective O–rich shell, where the radioactive nuclei, such as ^{56}Ni, are mainly synthesized. The other is that core collapse will amplify the initial fluctuation in the Fe core to the degree of $\delta R_s/R_s \sim$ 30%, where R_s is the shock radius (Burrows & Hayes 1995).

Another problem is the reproduction of the line profiles of heavy elements. The line profiles of Co and Fe have shown that a small fraction of them is expanding at 3000–4000 km s^{-1}. On the other hand, numerical simulations can produce Co and Fe with velocities of order 2000 km s^{-1} at most, even if the acceleration by the energy release of the radioactive nuclei is taken into account (Herant & Benz 1991; Herant & Benz 1992). Although they insist that premixing of ^{56}Ni will be necessary for the reproduction, the problem of the high-velocity heavy elements seems to be unresolved.

There is another approach to that solution. If the explosion itself is not spherically symmetric, the situation will change dramatically. There are some reasons for which we should take account of the asymmetry in supernova explosion. Among them is the well-known fact that most massive stars are rapid rotators (Tassoul 1978). It is well known that stars spin down as they evolve, especially through the red supergiant stage, losing their total angular momenta. However, pulsars found in supernova remnants are certainly rapidly rotating. This fact suggests that there is still a large angular momentum in the center region of the star when it collapses. Since stars are rotating in reality, the effect of rotation should be investigated in numerical simulations of a collapse-driven supernova. Thus far, several simulations have been done by a few groups in order to study rotating core collapse (Müller, Rozyczka, & Hillebrandt 1980; Tohline, Schombert, & Boss 1980; Müller &

[1] Department of Physics, School of Science, University of Tokyo, 7-3-1 Hongo, Bunkyoku, Tokyo 113, Japan.
[2] Institute of Physical and Chemical Research, Wako, Saitama, 351-01, Japan.
[3] Research Center for the Early Universe, Faculty of Science, University of Tokyo, 7-3-1 Hongo, Bunkyoku, Tokyo 113, Japan.

Hillebrandt 1981; Bodenheimer & Woosley 1983; Symbalisty 1984; Mönchmeyer & Müller 1989; Finn & Evans 1990; Yamada & Sato 1994). As a result, some numerical simulations of a collapse-driven supernova show the possibility of jetlike explosion if the effect of a stellar rotation and/or stellar magnetic field is taken into consideration. There is also a possibility that the axisymmetrically modified neutrino radiation from a rotating protoneutron star causes asymmetric explosion (Shimizu, Yamada, & Sato 1994). We note that these above-mentioned effects tend to cause axisymmetric explosion. In addition, axisymmetric explosion has an advantage in the explanation of some observational facts. For example, it is reported that axisymmetric explosion has the possibility of producing sufficient ^{44}Ti to explain the tail of the light curve of SN 1987A (Nagataki et al. 1997). Furthermore, some observations of SN 1987A suggest the asymmetry of the explosion. The clearest is the speckle images of the expanding envelope with high angular resolution (Papaliolis et al. 1989), where an oblate shape with an axis ratio of ~ 1.2–1.5 was shown. Similar results were also obtained from the measurement of the linear polarization of the scattered light from the envelope (Cropper et al. 1988). If the envelope is spherically symmetric, there is no net linear polarization induced by scattering. Assuming again that the shape of the scattering surface is an oblate or prolate spheroid, one finds that the observed linear polarization corresponds to an axis ratio of ~ 1.2. We must note that the observed nonspherical nature of the morphology in the radio remnant of SN 1987A can be explained by the circumstellar medium inhomogeneities, rather than by explosion asymmetry (Gaensler et al. 1996). However, this observation does not necessarily rule out the intrinsic asymmetric explosion. Because of these reasons mentioned above, it is important to investigate the effect of axisymmetric explosion on the mixing of the ejecta.

Based upon these facts, Yamada & Sato (1991) made two-dimensional hydrodynamical calculations for axisymmetric and equatorial-symmetric explosion. They found that heavy elements could be highly accelerated in an axisymmetric explosion and reach velocities of order of 4000 km s^{-1} when the amplitude of the initial instabilities is as large as $\sim 30\%$.

However, some points of their calculation can be improved, as mentioned below. First, they calculate matter mixing only with one model, that is, the initial velocity behind the shock wave is assumed to be proportional to $r \cos^2 \theta$, where θ is the zenith angle. This assumption is groundless and not persuasive. Second, although they show the presence of the high-velocity heavy elements in the calculation, they do not calculate line profiles of heavy elements, which should be compared to observations. Third, they assume that the chemical composition of the ejecta and the mass cut are spherically symmetric. Finally, since their numerical algorithm is constructed by the donner cell method, we find it necessary to ascertain their results with a more refined algorithm.

In this paper the degree of the axisymmetric explosion is changed parametrically, and the velocity distribution of heavy nuclei is calculated for each model. We will limit the degree of the axisymmetric explosion and the initial fluctuation by comparing the results with observations. In each calculation the results of explosive nucleosynthesis under the explosion are used for the chemical composition and mass cut (Nagataki et al. 1997). Moreover, Roe's scheme of second-order accuracy in space (Hirsch 1990; Shimizu 1995; Shimizu 1996) is adopted for the calculation.

We show our method of calculation for the matter mixing in § 2. Results are presented in § 3. A summary and discussion are given in § 4.

2. MODEL AND CALCULATIONS

2.1. *Hydrodynamics*

We performed two-dimensional hydrodynamical calculations. The calculated region corresponds to a quarter part of the meridian plane under the assumption of axisymmetry and equatorial symmetry. The number of meshes is 2000×100 (2000 in the radial direction and 100 in the angular direction). The size of radial meshes is arranged so as to increase as a geometrical series. Both the innermost radius and mesh size are set to be 10^8 cm. The outermost radius is set to be 3.3×10^{12} cm, that is, the surface of the progenitor. As for the algorithm, we use Roe's scheme of second-order accuracy in space. The basic equations are as follows:

$$\partial_t \rho = -\frac{1}{r^2}\,\partial_r(\rho u_r r^2) - \frac{1}{r \sin\theta}\,\partial_\theta(\rho u_\theta \sin\theta)\,, \tag{1}$$

$$\partial_t(\rho u_r) = -\frac{1}{r^2}\,\partial_r(\rho u_r^2 r^2) - \frac{1}{r\sin\theta}\,\partial_\theta(\rho u_r u_\theta \sin\theta) \tag{2}$$

$$- \partial_r P + \frac{\rho u_\theta^2}{r}\,, \tag{3}$$

$$\partial_t(\rho u_\theta) = -\frac{1}{r^2}\,\partial_r(\rho u_\theta u_r r^2) - \frac{1}{r\sin\theta}\,\partial_\theta(\rho u_\theta^2 \sin\theta) \tag{4}$$

$$-\frac{1}{r}\,\partial_\theta P - \frac{\rho u_\theta u_r}{r}\,, \tag{5}$$

$$\partial_t E = -\frac{1}{r^2}\,\partial_r[(E+P)u_r r^2] \tag{6}$$

$$-\frac{1}{\sin\theta}\,\partial_\theta[(E+P)u_\theta \sin\theta]\,, \tag{7}$$

where ρ, P, and E are the mass density, pressure, and total energy density per unit volume, respectively, and u_r and u_θ are velocities of a fluid in the r- and θ-direction, respectively. The first equation is the continuity equation, the second and third are the Euler equations, and the forth is the equation of the energy conservation. We use the equation of state,

$$P = \frac{1}{3}\,aT^4 + \frac{\rho k_{\mathrm{B}} T}{A_\mu m_u}\,, \tag{8}$$

where a, k_{B}, A_μ, and m_u are the radiation constant, Boltzmann constant, the mean atomic weight, and the atomic mass unit, respectively.

In this paper we assume that the system is adiabatic after the passage of the shock wave, because the entropy produced during the explosive nucleosynthesis is much smaller than that generated by the shock wave. This means the effect of the nickel bubble is not included in this study.

2.2. *Postprocessing*

In order to see how matter is mixed by R-T instabilities quantitatively, we use a test-particle approximation. We will explain this approximation.

First, test particles are put in the progenitor. It is assumed that test particles are at rest and scattered in the Si-rich and inner O-rich layers, where heavy radioactive elements are mainly synthesized by the explosive nucleosynthesis, with the same interval in the radial and angular directions in each layer. We put $10(r) \times 100(\theta)$ particles in each layer. In additional, we put $10(r) \times 100(\theta)$ particles in outer O-, He-, and H-rich layers in the same way. The initial positions of test particles are summarized in Table 1.

In calculating the degree of mixing, we assume that each test particle has its own mass, which is determined by the initial distribution of the test particles so that their sum becomes the mass of the Si-, O-, He-, and H-rich layers, and we also assume that each test particle has its own composition, which is determined by the calculation of explosive nucleosynthesis. We use the results of Nagataki et al. (1997, hereafter NHSY) for the composition, as stated below.

It is assumed that test particles are at rest at the beginning ($t = 0$). We also assume that they move with the local velocity at their positions after the passage of a shock wave. Thus, we can calculate each particle's path by integrating $\partial \boldsymbol{x}/\partial t = \boldsymbol{v}(t, x)$, where the local velocity $\boldsymbol{v}(t, x)$ is given from the hydrodynamical calculations. In this way we can calculate the degree of the mixing quantitatively and can calculate the velocity distribution of each element, such as ^{56}Ni, at each time.

2.3. *Hydrodynamical Initial Condition*

First, we will explain the initial shock wave. Since there is still uncertainty as to the mechanism of Type II supernovae, all calculations of matter mixing have not been performed from the beginning of the core collapse. Instead, explosion energy is deposited artificially at the innermost boundary (e.g., Hachicu et al. 1992). In this paper this method is chosen, and the explosion energy of 1.0×10^{51} ergs is injected to the region from 1.0×10^8 to 1.5×10^8 cm (that is, at the Fe/Si interface).

As for the axisymmetric explosion, the initial velocity of matter behind the shock wave is assumed to be radial and proportional to $r(1 + \alpha \cos 2\theta)/(1 + \alpha)$, where r, θ, and α are the radius, the zenith angle, and the free parameter, which determines the degree of the axisymmetric explosion, respectively. Since the ratio of the velocity in the polar region to that in the equatorial region is $1:(1 - \alpha)/(1 + \alpha)$, more extreme jetlike shock waves are obtained as α gets larger. In the present study we take $\alpha = 0$ for the spherical explosion and $\alpha = \frac{1}{3}$, $\frac{3}{5}$, and $\frac{7}{9}$ (these values mean that the ratios of the velocity are 2:1, 4:1, and 8:1, respectively) for the axisymmetric explosions (see Table 2). We assumed that the distribution of thermal energy is the same as the velocity distribution and that the total thermal energy is equal to the total kinetic energy.

Next, in order to see the evolution of the fluctuation, we must introduce perturbation artificially. From the linear stability analysis, the linear growth rate is given as (Chankrasekhar 1981)

$$G_{\rm RT}^2 = \frac{\rho_+ - \rho_-}{\rho_+ + \rho_-} k g_{\rm eff} , \tag{9}$$

where ρ_+, ρ_-, k, and $g_{\rm eff}$ are the densities in the upper and lower layers, the wavenumber of the density perturbation, and effective gravity, respectively. In our calculation, the effective gravity is nearly equal to $-dP/\rho\, dr$.

As one can see from the growth rate, perturbations of shorter wavelengths grow faster than those of longer ones. So, the power spectrum of density perturbation of a star is very important information. However, this power spectrum has not been found from observations. Only some numerical simulations of the progenitor predict the spectrum (Bazan & Arnett 1994, 1997). Moreover, numerical calculations inherently introduce some amount of viscosity that suppresses the growth of instabilities of wavelengths shorter than a certain value, which would grow at the fastest rate, if such perturbations actually exist. We must keep in mind that numerical calculations of R-T instabilities in a star have the uncertainties mentioned above.

Historically speaking, there are two ways of introducing perturbations. One is by the periodic method, and the other is by the random perturbation method. In the periodic perturbation method, a growing mode is given a priori; characteristic wavelength is not given in the random perturbation method. A form of power spectrum is assumed in these methods; there is no guarantee that a real star has such a form.

In this paper we chose a periodic perturbation method, considering it to be better rather than random perturbation since we are interested in the different growth rates in different directions (Yamada & Sato 1991) under the same fluctuation pattern. As many have done, we perturb only the velocity field inside the shock wave when the shock front reaches the He/H interface. When we calculate the axisymmetric explosion, we introduce perturbation when the shock front in the polar region reaches that interface. We adopt monochromatic perturbations, i.e., $\delta v = \varepsilon v(r, \theta) \cos m\theta$ ($m = 20$). In this paper we performed calculations with three values of perturbations, that is, 0%, 5%, and 30% were taken for the value of ε. These model parameters are summarized in Table 3. We note that it is reported that the mixing width, i.e., the length of the mushroomlike "fingers," depends only slightly on the mesh resolution when ε is larger than $\sim 5\%$ of the expansion speed (Hachicu et al. 1992). For this reason we think that the influence of the power spectrum of the initial perturbation is relatively small in this study.

We note that the form of the initial shock wave and the degree of the initial fluctuation cannot be known directly. Rather, we will attempt to limit these initial conditions by

TABLE 1

Initial Positions of Test Particles

Radius (cm)	Number
$(1.5–3.0) \times 10^8$	1000
$(3.0–9.0) \times 10^8$	1000
$9.0 \times 10^8–6.3 \times 10^9$	1000
$6.3 \times 10^9–4.8 \times 10^{10}$	1000
$4.8 \times 10^{10}–3.3 \times 10^{12}$	1000

TABLE 2

Models for the Initial Shock Wave

Model	S1	A1	A2	A3
α	0	1/3	3/5	7/9
$V_p:V_e$[a]	1:1	2:1	4:1	8:1

[a] Ratio of the velocity in the polar region ($\theta = 0°$) to that in the equatorial region ($\theta = 90°$).

TABLE 3

MODELS, VALUES OF α, AND PERTURBATION AMPLITUDES

Model	α	Perturbation (%)	Model	α	Perturbation (%)
S1a	0	0	A2a	3/5	0
S1b	0	5	A2b	3/5	5
S1c	0	30	A2c	3/5	30
A1a	1/3	0	A3a	7/9	0
A1b......	1/3	5	A3b	7/9	5
A1c	1/3	30	A3c	7/9	30

comparing the results with observations under the assumption of periodic perturbation.

2.4. *Progenitor, Chemical Composition, and Mass Cut*

The progenitor of SN 1987A, Sk-69°202, is thought to have had a mass of $\sim 20\ M_\odot$ in the main-sequence stage (Shigeyama, Nomoto, & Hashimoto 1988; Woosley & Weaver 1988) and a $\sim 6 \pm 1\ M_\odot$ helium core (Woosley 1988). Thus, for the initial density of the progenitor we use the presupernova model that is obtained from the evolution

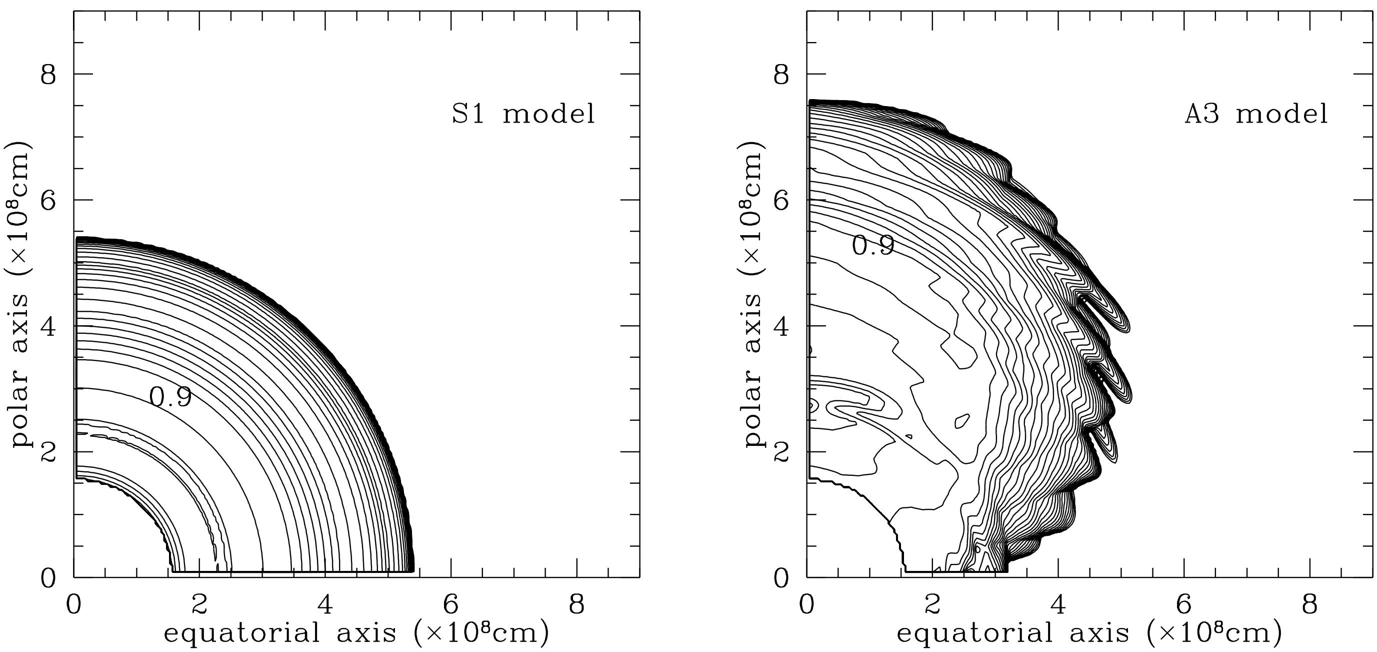

FIG. 1.—*Left*: Contour of the mass fraction of ^{56}Ni in model S1. The maximum value of the mass fraction of ^{56}Ni is 9.3×10^{-1}. The region in which the mass fraction of ^{56}Ni becomes 0.9 is noted in the figure. *Right*: Same as left, but for model A3. The maximum value is 9.1×10^{-1}. Contours are drawn for the initial position of test particles.

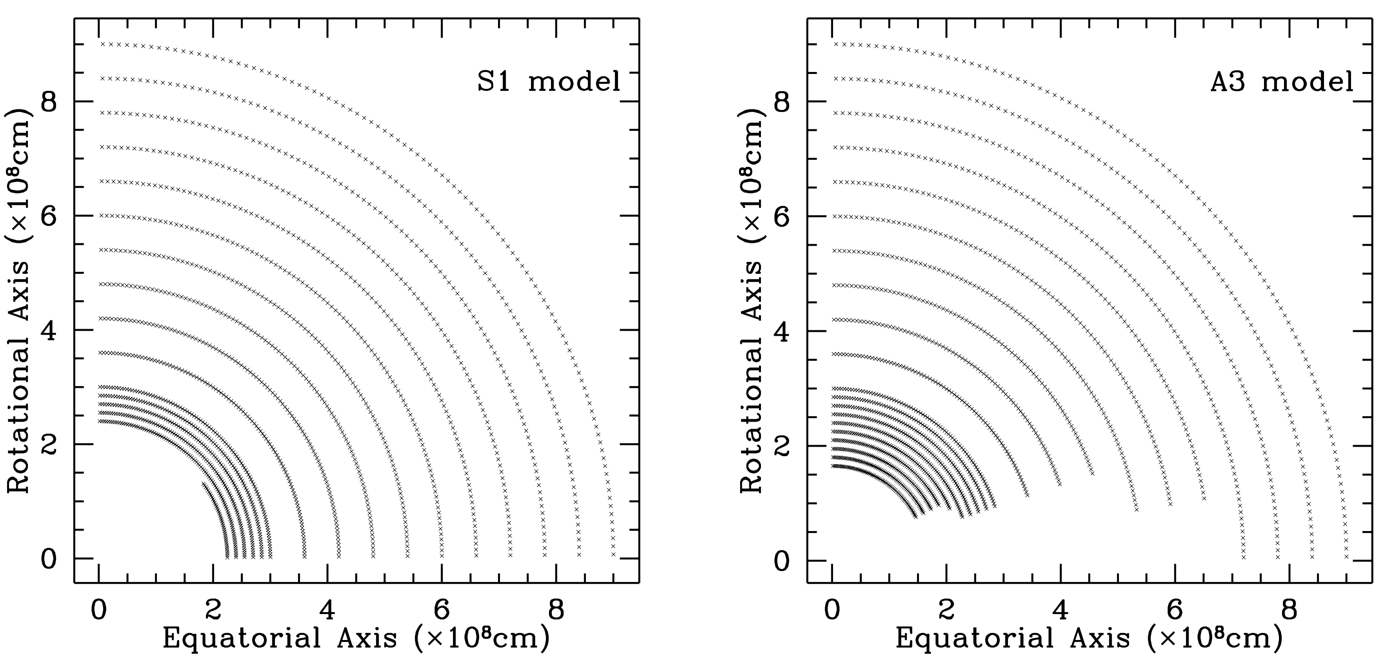

FIG. 2.—Form of the mass cut for models S1 and A3. Dots are plotted for the initial positions of the test particles that will be ejected.

of a helium core of 6 $M_\odot$ (Nomoto & Hashimoto 1988), and its hydrogen envelope. The total mass of the progenitor corresponds to 16.3 $M_\odot$.

The chemical composition of the progenitor is changed by nuclear burning when the shock wave passes (explosive nucleosynthesis). We used the results of NHSY for the explosive nucleosynthesis. For example, in Figure 1 we show the contour of the mass fraction of ^{56}Ni for models S1 and A3. We note that this effect of the initial asymmetric chemical composition has never been considered in previous studies.

For the mass cut we use the results of NHSY. In Figure 2 we show the mass cuts for models S1 and A3. These mass cuts are chosen so as to contain 0.07 $M_\odot$ of ^{56}Ni in the ejecta. However, we must note that defining the form of the mass cut is a very difficult problem, since it is sensitive not only to the explosion mechanism, but also to the presupernova structure, stellar mass, and metallicity (Woosley & Weaver 1995). Moreover, the form of the mass cut has a large influence on the mixing of ^{56}Ni since, it is mainly produced near the mass cut. For these reasons, we must investigate the sensitivity of the results to the mass cut (see § 3.2).

3. RESULTS

3.1. *Global Density Structure and Position of* ^{56}Ni

In this paper 12 models are made in all. We show the density contours of S1b at time $t = 5000$ s in Figure 3. Mushroomlike "fingers," which are characteristic of the nonlinear growth of R-T instability, can be seen in this model. This is consistent with the work of other groups (e.g., Fryxell et al. 1991; Hachicu et al. 1992). From this point of view, we think that the resolution of our calculations is high enough to show the global behavior of the matter mixing.

Next, positions of test particles are shown at time $t = 5000$ s for S1b and S1c in Figure 4. For comparison, we show these for A3b and A3c in Figure 5. As expected, the matter is mixed more in the larger initial perturbation models (models S1c and A3c). We can also see that the matter is mixed more in the polar region than in the equatorial region for the axisymmetric explosion models (models A3b and A3c).

We must also comment on the effect of two-dimensional calculations. All calculations presented here are performed in two dimensions so as to save the computer's CPU time and memory and to allow the extensive exploration of the parameter space carried out in this study. Readers should note here that there is a tendency in three-dimensional modes of growing to higher mixing velocities than in two-

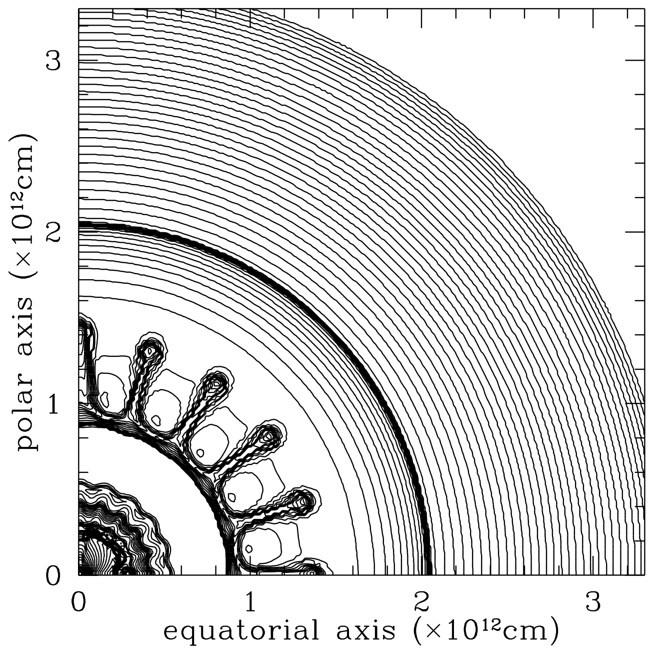

FIG. 3.—Density contour for model S1b at $t = 5000$ s. The shock wave can be seen at the radius $\sim 2 \times 10^{12}$ cm. The growth of R-T instabilities can be seen inside the shock wave.

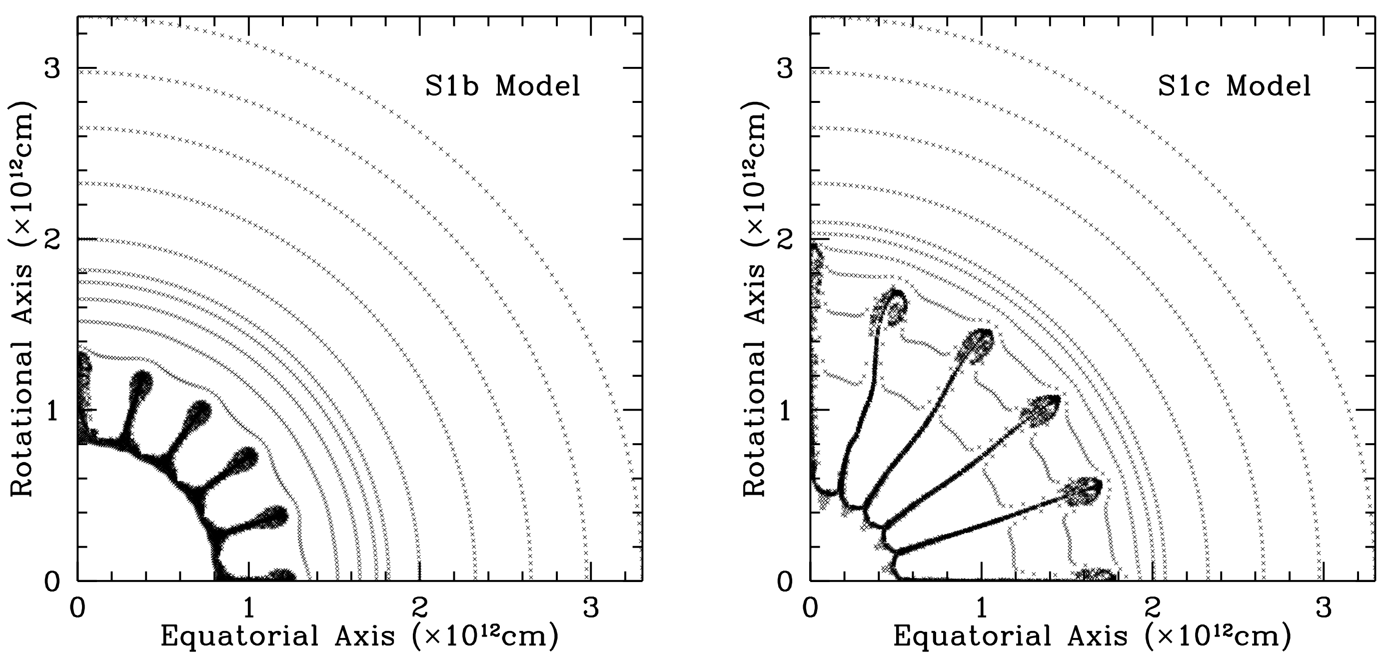

FIG. 4.—Positions of test particles at time $t = 5000$ s after explosion. *Left:* Model S1b; *right:* model S1c.

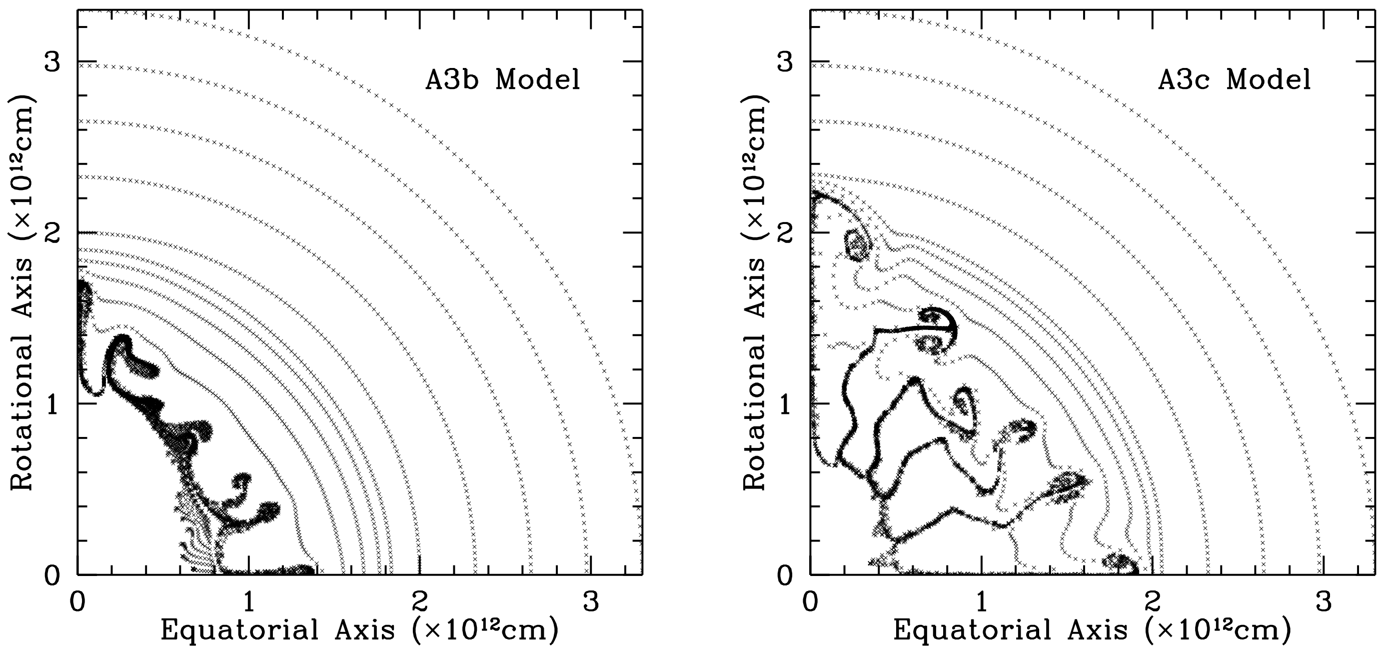

FIG. 5.—Same as Fig. 4, but for models A3b and A3c

dimensional modes (Remington et al. 1991; Yabe 1991; Marinak et al. 1995). This seems to be the reason why the finger at the $\theta = 0°$ axis is further along than at the $\theta = 90°$ axis, even in the spherical explosion model S1c. However, three-dimensional simulations of the explosion of SN 1987A (Müller et al. 1990) have shown little change in relation to the two-dimensional case. Moreover, in comparing Figures 4 and 5, we think that the effect of axisymmetric explosion is quite large, compared to the two-dimensional effect. It is true that the three-dimensional effect should be investigated with high resolution in the future, but we think our quantitative estimates discussed below are not unreasonable.

3.2. *Velocity Distribution of* ^{56}Ni

We will pay attention to ^{56}Ni, which is responsible for the behavior of the bolometric light curve, the early detection of X-rays and gamma rays, and their light curves.

First, we investigate the velocity distributions of ^{56}Ni for all models. Figures 6 and 7 represent these results. We can see that the range of velocity gets wider as the initial perturbation gets larger for any explosion model, that is, irrespective of the value of α. However, high-velocity ^{56}Ni of order 3000–4000 km s^{-1} cannot be produced in the spherical explosion case, even if the initial perturbation is as large as 30%. On the other hand, such high-velocity ^{56}Ni is produc-

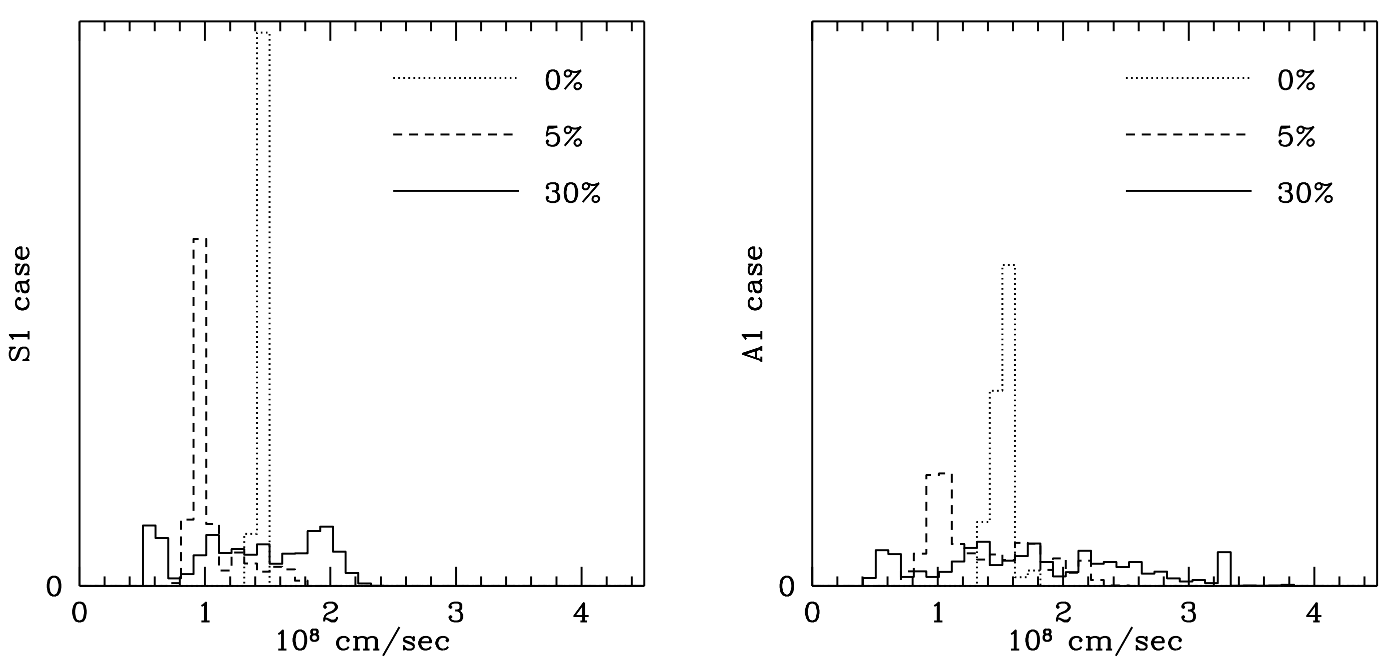

FIG. 6.—Velocity distribution of ^{56}Ni at time t = 5000 s after explosion. *Left:* Model S1; *right:* model A1.

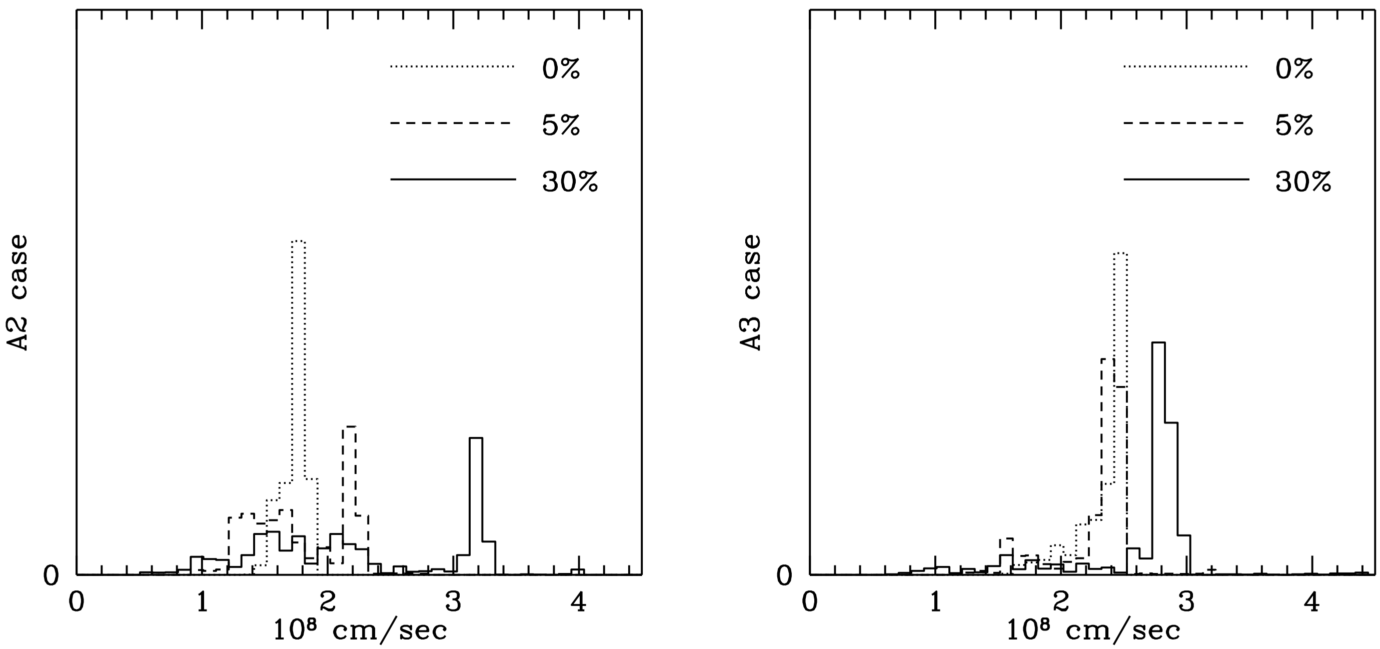

FIG. 7.—Same as Fig. 6, but for models A2 and A3

ed for any axisymmetric explosion for the case of 30% initial perturbation. However, too much high-velocity ^{56}Ni seems to be produced for the strong axisymmetric explosion case (see models A2c and A3c in Fig. 7). This might be a constraint for the degree of axisymmetric explosion. We will investigate this suggestion more carefully in what follows.

Before we continue to further discussion, we would like to comment on the average velocity of ^{56}Ni. In the perturbed models the lower velocity component and the higher velocity component appear naturally, compared to the no-perturbation models, since monochromatic perturbation is given. As ϵ becomes large, its degree also becomes large. In fact, it can be seen in Figures 4 and 5 that the radius of the innermost layer is smaller in the 30% models, compared to the 5% models. At the same time the mixing width is larger in the 30% models. In other words, it seems that the ram pressure caused by ingoing bubbles of lighter elements suppresses the bulk velocity of heavy elements, while part of the latter is accelerated by the outgoing mushrooms. The average velocity of ^{56}Ni is determined by how much ^{56}Ni is taken in the mushroom and how much ^{56}Ni remains in the innermost region. As a consequence, the average velocity of ^{56}Ni does not necessarily grow higher with ϵ. In fact, we can see in Figure 6 that the average velocity of ^{56}Ni becomes lower in the 5% models, compared to the no-perturbation models.

Next, we calculate line profiles for optically thin ejecta and compare them to observations in order to examine the suggestion mentioned above. However, the interpretation of calculated line profiles is complicated by the line of sight of the observer. The symmetry axis inferred from the observation of the ring of SN 1987A (Plait et al. 1995) is different from that inferred from the speckle interferometry (Papaliolis et al. 1989). In this paper we calculate line profiles seen from $\theta = 44°$, which is inferred from the ring of SN 1987A. The results are shown in Figures 8 and 9. For comparison, observed infrared line profiles of Fe from SN 1987A are shown in Figure 10. As for the spherical explosion, high-velocity elements cannot be seen. On the other hand, as α gets large, the form of the line profile becomes different from that of observations. In particular, it is unlikely that the strong axisymmetric explosion model (the $\alpha = \frac{3}{5}$, $\frac{7}{9}$ case) can reproduce the line profile. We can say that model A1c most closely resembles the line profile including the high-velocity element.

Finally, as mentioned in § 2.4, we must examine the sensitivity of our results for the mass cut. We can easily guess that the low-velocity element will grow larger if the mass cut is assumed to be spherical, since the velocity is small near the equatorial region, which is cut by the asymmetric mass cut. We show line profiles incorporating the spherical mass cut for comparison in Figures 11 and 12. As expected, the enhancement of the small-velocity element is seen. However, models A2c and A3c are still far from the observed line profile. From this result, we find models A2 and A3 to be rejected by observations. On the other hand, model A1c begins to resemble observations, supporting the proposal that it can reasonably reproduce them. We also performed a simulation in order to investigate the effect of asymmetric explosive nucleosynthesis (Nagataki et al. 1997) on the velocity distribution of ^{56}Ni. It is found, however, that the effect of the asymmetric mass cut is of much greater importance.

3.3. *Minimum Velocity of Hydrogen*

Additionally, we see the minimum velocity of hydrogen. These results are summarized in Table 4. We can identify the tendency for the minimum velocity to become lower as the degree of axisymmetric explosion gets larger when the initial perturbation is set at zero. It is also seen that as the initial perturbation amplitude is increased, the minimum velocity decreases for the same degree of axisymmetric explosion. However, we cannot say that the minimum velocity decreases as the degree of axisymmetric explosion and initial perturbation are both increased. Although we cannot explain the reason clearly, we can say that all

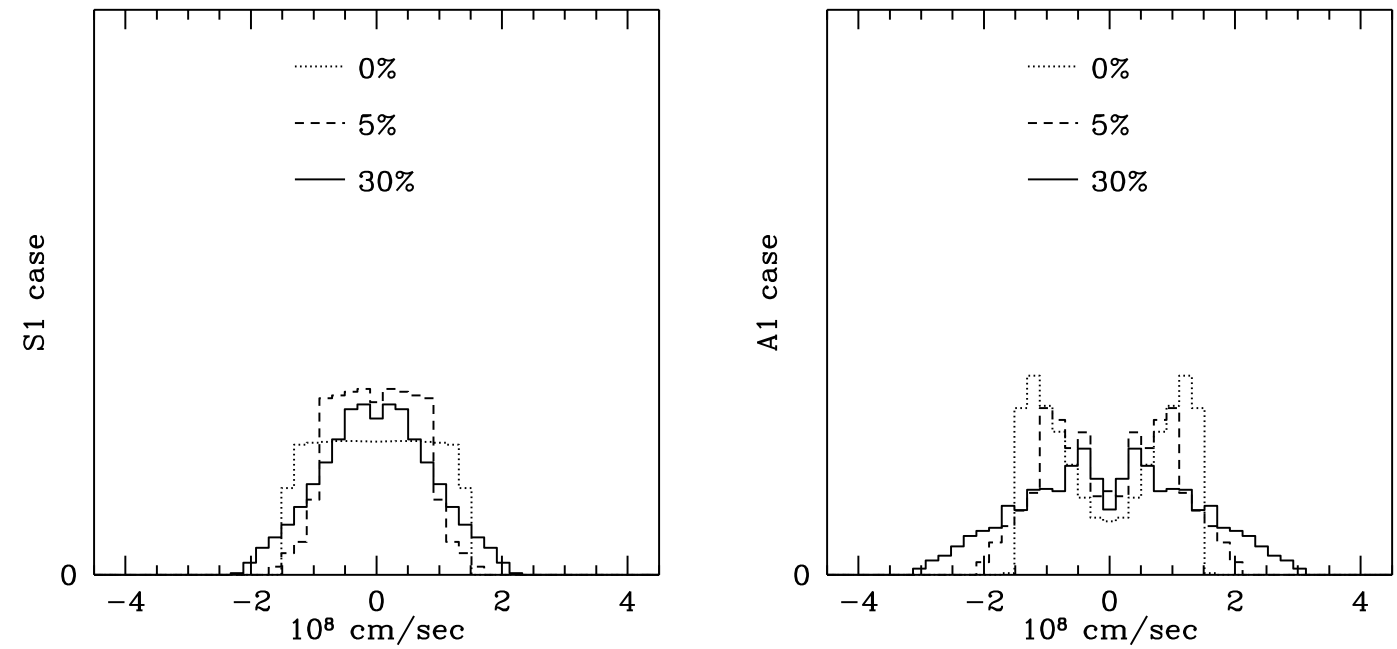

FIG. 8.—Line profile of ^{56}Ni seen from $\theta = 44°$ at time $t = 5000$ s after explosion. *Left:* Model S1; *right:* model A1.

TABLE 4

MINIMUM VELOCITY OF HYDROGEN AT TIME $t = 5000$ s

Amplitude of Initial Perturbation	S1	A1	A2	A3
0%	1.6	1.5	1.3	1.1
5%	0.87	0.89	0.86	0.90
30%	0.85	0.53	0.57	0.76

NOTE.—In units of 10^8 cm s^{-1}.

models that have an initial perturbation greater than 5% can explain observation, which shows a minimum velocity of hydrogen $\sim$800 km s^{-1}.

4. SUMMARY AND DISCUSSION

We have performed a two-dimensional hydrodynamic calculation for an axisymmetric explosion with a periodic perturbation. The degree of the explosion axisymmetry is varied and three perturbation amplitudes are studied for each explosion. We have compared calculated line profiles to observations, with special attention paid to the high-velocity element. Limits on initial perturbation amplitude and degree of axisymmetry are established based on our comparison.

We find the high-velocity element cannot be produced for

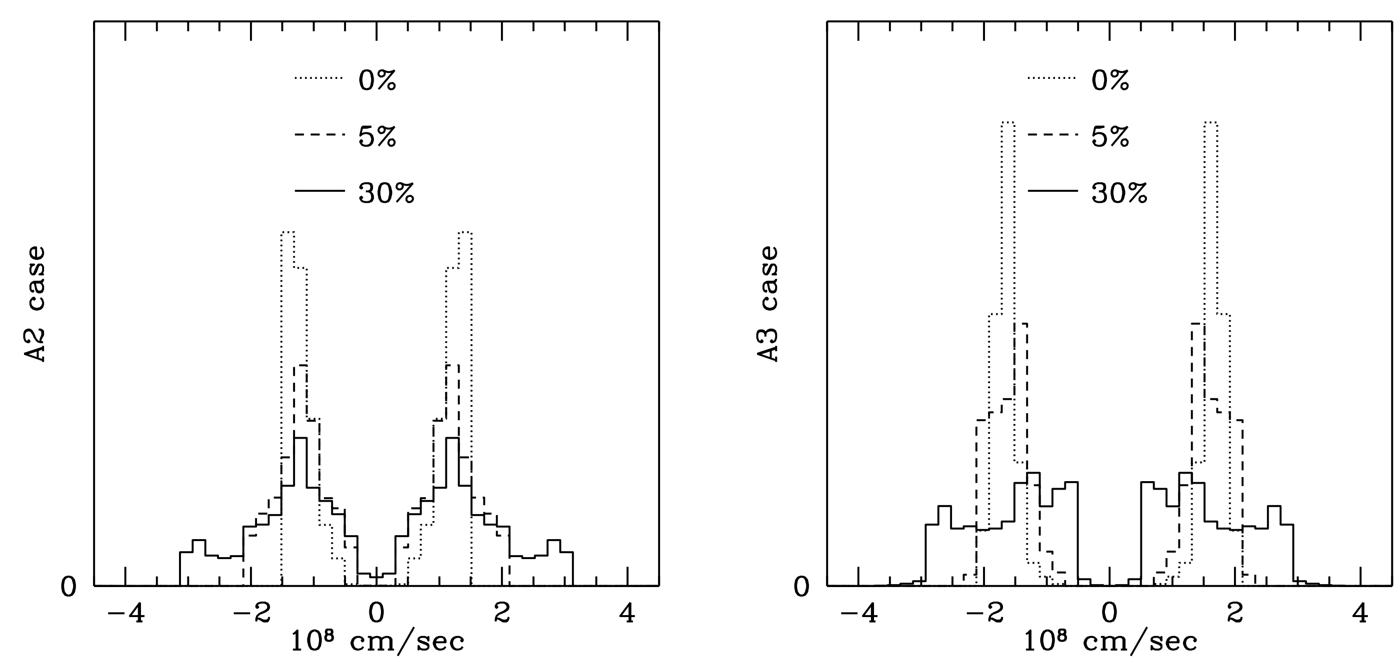

FIG. 9.—Same as Fig. 8, but for models A2 and A3

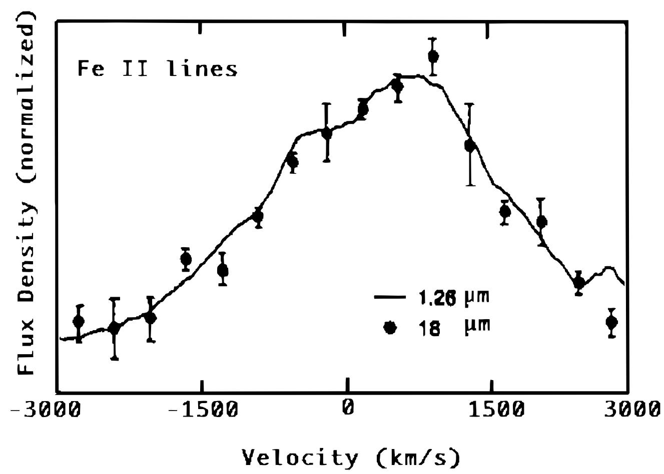

FIG. 10.—Observed infrared line profiles for Fe at 1.26 μm (*solid line:* $t = 377$ days; Spyromilio, Meikle, & Allen 1990) and at 18 μm (*data points*, $t = 407$ days; Haas et al. 1990). Positive velocities (km s^{-1}) correspond to a redshift.

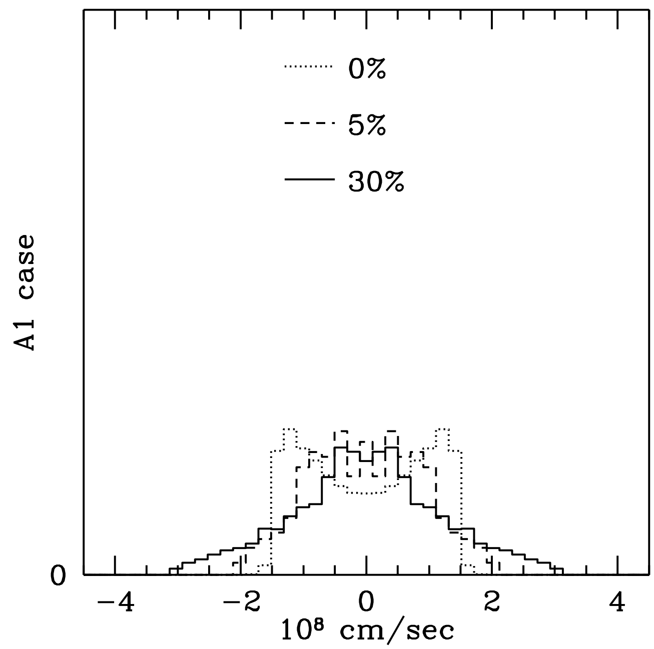

FIG. 11.—Line profile of ^{56}Ni for model A1, seen from $\theta = 44°$ at time $t = 5000$ s after explosion under the spherical mass cut.

any spherical explosion model, even if the initial perturbation amplitude is as large as 30%. On the other hand, it is produced by the axisymmetric explosion, if the initial perturbation amplitude is 30%. As for the origin of the perturbation, we cannot attribute such a large perturbation ($\sim$30%) to the structure of the progenitor (Bazan & Arnett 1994; Bazan & Arnett 1997). We feel that only the dynamics of the core-collapse explosion itself can lead such a large perturbation. However, we must note that if other mechanisms, such as nickel bubbles, work effectively, the required amplitude will be less than 30%. We also note another possible source of a large perturbation: the offset of the core from the center of mass of the star. This is being studied now by P. Goldreich as the effect of gravity waves from convective zones acting in constructive interference as they converge toward the core. This leads to some oscillatory behavior of the core about the center of mass. However, the amplitude of the perturbation generated by this effect has not yet been reported.

The line profiles also serve as upper limits for the degree of explosion axisymmetry. Line profiles are affected by the presence of a mass cut. However, models A2c and A3c cannot reproduce the observed line profile, even if different mass cut positions are incorporated. We think that this

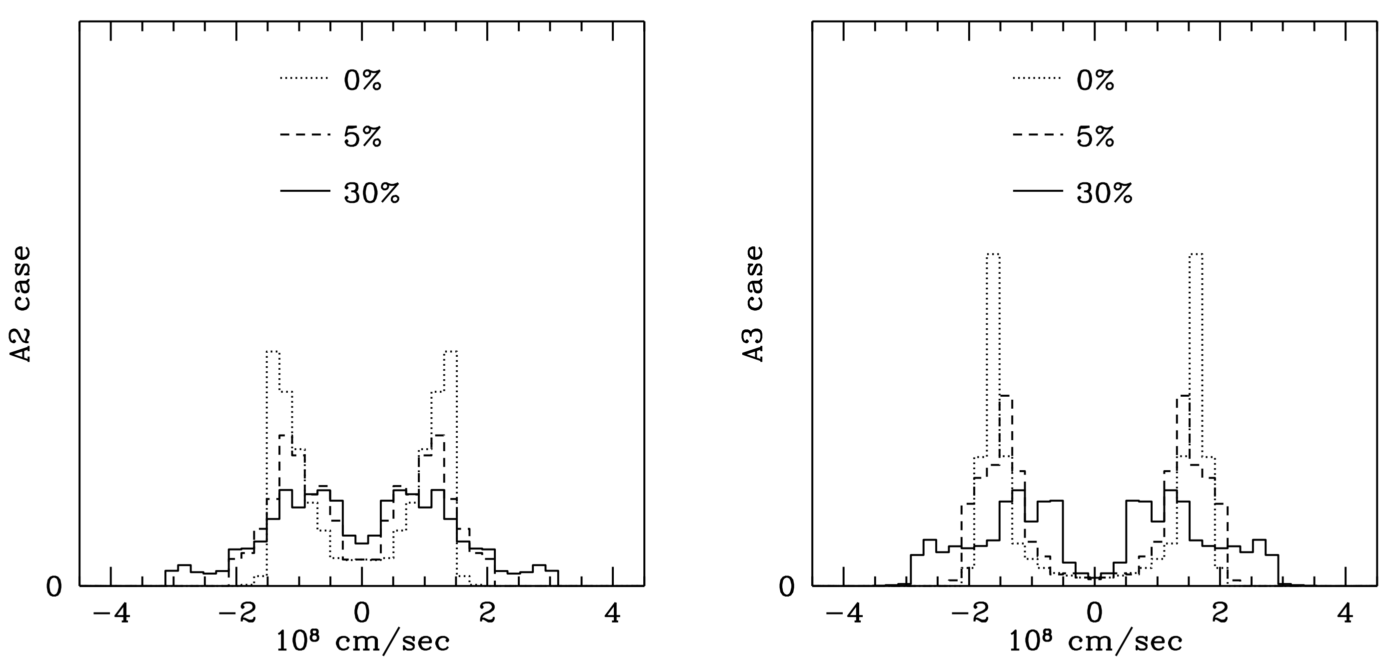

FIG. 12.—Same as Fig. 11, but for models A2 and A3

provides an upper limit to the degree of the axisymmetric explosion. This fact will be important for simulations of collapse-driven supernovae including rotation, magnetic field, and axisymmetric neutrino radiation.

On the other hand, the weak axisymmetric model A1c best reproduces the observations, including the high-velocity element. Since the line profile is also changed by the angle between our line of sight and polar axis and by the radiative transfer, the information provided by the line profile is ambiguous. We can only say that there is an axisymmetric explosion model that can reproduce the line profile.

To provide an additional constraint, we calculated the lowest velocity of hydrogen. The results showed that any explosion model can explain the observed value ~ 800 km s^{-1} if the amplitude of the initial perturbation is larger than 5%.

We must note that our results are obtained on the assumption of the periodic perturbation method. As stated in § 2.3, the effect of the initial power spectrum of density perturbations should be explored in future. In particular, it will be important to perform R-T calculations using the asymmetric progenitor models (Bazan & Arnett 1994, 1997), since these two-dimensional models predict the power spectrum of density perturbations. The models may also hold a key to the reproduction of the observed line asymmetry, such as that of Figure 10. However, we think that the influence of the power spectrum of the initial perturbation is relatively small in this study, since the amplitudes of initial perturbations are larger than 5% of the expansion speed (Hachicu et al. 1992).

We also note the effect of the Coriolis force. When the instabilities of other targets with sufficient angular velocity, such as an accretion disk around a black hole, are explored (Ruffert & Arnett 1994), the Coriolis force will play an important role in the growth of instabilities. However, we neglected the rotation of the mantle and envelope in this paper, since the rotation velocity is much smaller than the explosion velocity where the R-T instabilities grow.

We will consider the reliability of our calculations. Grid resolution is relevant, since higher resolution can reproduce better the steep gradients of physical quantities such as density, pressure, and temperature. Fryxell, Müller, and Arnett have shown that the minimum resolution required for a "converged" model is determined by the hydrodynamic algorithm, and that there is a possibility that numerical errors might dominate the physical instability in much work that has already been done. On the other hand, Hachisu et al. (1990, 1992) have shown that the mixing width is insensitive to resolution in their Roe's third-order total variation diminishing (TVD) scheme, if the initial amplitude of the velocity perturbation is larger than 1% of the local sound speed (Hachicu et al. 1992). It is certainly important to see the structure of the mushrooms in detail, but our main purpose is to see the global behavior of the material. We think that our calculations have sufficient resolution for that purpose. For example, we can see the mushroomlike "finger" in the S1b case. Since the finger cannot be seen clearly in Yamada & Sato 1991 under the same conditions, but can be seen in other work (e.g., Hachicu et al. 1992), we conclude that our method is an improvement over that of Yamada & Sato 1991 and that our axisymmetric explosion models have sufficient resolution to describe the global behavior of the material accurately.

S. N. is grateful to S. Yamada for a useful discussion. We thank G. Bazan for his kind comments and review of this manuscript. S. N. and T. M. S. are a Junior Research Associate (JRA) member and a Special Postdoctoral Researcher at The Institute of Physical and Chemical Research (RIKEN), respectively. This work is supported in part by Grants-in-Aid from the Ministry of Education, Science and Culture of Japan (07CE2002, 07640386, and 07304033).

REFERENCES

Arnett, W. D., Fryxell, B. A., & Muller, E. 1989, ApJ, 341, L63
Bandiera, R. 1984, A&A, 139, 368
Bazan, G., & Arnett, W. D. 1994, ApJ, 433, L41
———. 1997, astro-ph/9702239
Bodenheimer, P., & Woosley, S. E. 1983, ApJ, 269, 281
Burrows, A., & Hayes, J. 1995, ApJ, 450, 830
Chandrasekhar, S. 1981, Hydrodynamic and Hydromagnetic Stability (New York: Dover)
Chevalier, R. A. 1976, ApJ, 207, 872
Cropper, M., Bailey, J., McCowage, J., Cannon, R. D., Couch, W. J., Walsh, J. R., Strade, J. O., & Freeman, F. 1988, MNRAS, 231, 695
Dotani, T., et al. 1987, Nature, 330, 230
Erickson, E. F., Haas, M. R., Colgan, S. W. J., Lord, S. D., Burton, M. G., Wolf, J., Hollebach, D. J., & Werner, M. 1988, ApJ, 330, L39
Falk, S. W., & Arnett, W. D. 1973, ApJ, 180, L65
Finn, L. S., & Evans, C. R. 1990, ApJ, 351, 588
Fryxell, B., Arnett, W. D., & Müller, E. 1991, ApJ, 367, 619
Gaensler, B. M., et al. 1997, ApJ, in press
Haas, R., Colgan, J., Erickson, F., Lord, D., Burton, G., & Hollenbach, J. 1990, ApJ, 360, 257
Hachisu, I., Matsuda, T., Nomoto, K., & Shigeyama, T. 1990, ApJ, 358, L57
———. 1992, ApJ, 390 230
Herant, M., & Benz, W. 1991, ApJ, 370, L81
———. 1992, ApJ, 387, 294
Hirsch, C. 1990, Numerical Computation of Internal and External Flows (Chichester: John Wiley)
Höflich, P. 1988, Proc. Astr. Soc. Australia, 7, 434
Itoh, M., Kumagai, S., Shigeyama, T., Nomoto, K., & Nishimura, J. 1987, Nature, 330, 233
Kumagai, S., Itoh, M., Shigeyama, T., Nomoto, K., & Nishimura, J. 1988, A&A, 197, L7
Marinak, M. M., et al. 1995, Phys. Rev. Lett, 75, 3677
Matz, S. M., Share, G. H., Leising, M. D., Chupp, E. L., Vestrand, W. T., Purcell, W. R., Strickman, M. S., & Reppin, C. 1988, Nature, 331, 416
Mönchmeyer, R. M., & Müller, E. 1989, in Timing Neutron Stars, PS49, ed. H. Ögelman & E. P. J. van den Heuvel (New York: ASI), 549
Müller, E., & Hillebrandt, W. 1981, A&A, 103, 358
Müller, E., Rozyczka, M., & Hillebrandt, W. 1980, A&A, 81, 288
Müller, E., Fryxell, B. A., & Arnett, W. D. 1990, in The Chemical and Dynamical Evolution of Galaxies, ed. F. Ferrini, F. Matteucci, & J. Franco (Pisa: Editrice Giardini)
———. 1991, A&A, 251, 505
Nagataki, S., Hashimoto, M., Sato, K., & Yamada, S. 1997, ApJ, 486, 1026
Nomoto, K., & Hashimoto, M. 1988, Phys. Rep., 163, 13
Papaliolis, C., Karouska, M., Koechlin, L., Nisenson, P., Standley, C., & Heathcote, S. 1989, Nature, 338, 13
Plait, P., Lundqvist, P., Chevalier, R., & Kirshner, R. 1995, ApJ, 439, 730
Remington, B. A., et al. 1991, Phys. Rev. Lett., 67, 3259
Ruffert, M., & Arnett, W. D. 1994, ApJ, 427, 351
Shigeyama, T., Nomoto, K., & Hashimoto, M. 1988, A&A, 196, 141
Shimizu, M. T. 1995, Ph.D. thesis, Univ. Tokyo
———. 1996, RIKEN Rev., 14, 27
Shimizu, M. T., Yamada, S., & Sato, K. 1994, ApJ, 432, L119
Spyromilio, J., Meikle, S., & Allen, A. 1990, MNRAS, 242, 669
Sunyaev, R. A. 1987, Nature, 330, 227

Symbalisty, E. M. D. 1984, ApJ, 285, 729
Tassoul, J. L. 1978, Theory of Rotating stars (Princeton: Princeton Univ. Press)
Tohline, J. E., Schombert, J. M., & Boss, A. P. 1980, Space Sci. Rev., 27, 555
Wilson, R. B., et al. 1988, in Nuclear Spectroscopy of Astrophysical Sources, ed. N. Gehrels & G. Share (New York: AIP), 66
Woosley, S. E. 1988, ApJ, 330, 218
Woosley, S. E., & Weaver, T. A. 1988, Phys. Rep., 163, 79
———. 1995, ApJS, 101, 181
Yabe, T. 1991, Numer. Astrophys. Japan, 2, 247
Yamada, S., & Sato, K. 1991, ApJ, 382, 594
———. 1994, ApJ, 434, 268